Polarization spectroscopy of dressed four-wave mixing in a three-level atomic system

Ruimin Wang,[1,3] Yigang Du,[1] Yanpeng Zhang,[1,4] Huaibin Zheng,[1] Zhiqiang Nie,[1] Changbiao Li,[1] Yuanyuan Li,[1] Jianping Song,[1] and Min Xiao[2]

[1]*Key Laboratory for Physical Electronics, Devices of the Ministry of Education & Shaanxi Key Lab of Information Photonic Technique and School of Science, Xi'an Jiaotong University, Xi'an 710049, China*
[2]*Department of Physics, University of Arkansas, Fayetteville, Arkansas 72701, USA*
[3]*wangrm@mail.xjtu.edu.cn*
[4]*ypzhang@mail.xjtu.edu.cn*

Received June 23, 2009; accepted July 16, 2009;
posted July 22, 2009 (Doc. ID 113174); published August 14, 2009

Polarization properties of pure four-wave mixing (FWM) and dressed-FWM processes in a two-level system and a cascade three-level atomic system are theoretically and experimentally investigated. The relative intensities and polarization characteristics of the FWM signals in different laser polarization configurations and different level systems are experimentally investigated and compared. Also, the results are theoretically explained by different transition paths combinations. In the dressed-FWM processes, we study the dependence of dressing effect on the incident field's polarization. The FWM signal generated by a linearly polarized pumping field is suppressed more by the dressing field than the one generated by a circularly polarized pumping field. However, an opposite effect was observed when the probe field's polarization is changed. The multidressing mechanisms are used to explain these effects. In addition, the interference and polarization dependence of the coexisting FWM signals in the same atomic system are discussed.

OCIS codes: 190.4380, 270.4180, 300.2570, 320.7110, 030.1670.

1. INTRODUCTION

The parametric four-wave mixing (FWM) is a useful process for generating coherent radiations from vacuum ultraviolet to infrared wavelengths. The polarization characteristics of two-photon resonant FWM processes have been investigated in several types of metal vapors gases. Tsukiyama [1] described polarization properties of the near-infrared FWM signal produced in Kr vapor, Museur *et al.* [2] studied the polarization dependence of the vacuum ultraviolet light generated by a four-wave sum-frequency generation process in Hg, and Ishii *et al.* [3] investigated polarization characteristics of FWM in NO gas. Besides producing coherent emissions, parametric FWM processes can also be used to study interference effects. Previous studies have used FWM processes to observe interference effects between different atomic polarizations [4–6]. Studies of interference effects in multilevel atomic systems have become an active field of research in recent years, which made it possible to coherently control the optical properties of atomic media [7,8]. In parametric FWM processes, there are multiple quantum paths for each step of the nonlinear processes, and the probability amplitudes for these different transition paths are intimately related to the polarizations of the input laser fields. Therefore, it is possible to coherently control the nonlinear processes by manipulating the polarization states of incident laser beams.

In this paper, we report both theoretical and experimental results on the polarization dependence of the FWM signals generated in Na atomic vapor. Both two-level and three-level systems in Na atoms are used in these studies. The classical, as well as quantum, theoretical models have been developed to explain the dependence of the FWM signals on the polarization states of the incident laser beams. By comparing the FWM spectra for different laser polarization configurations, we can identify different contributions from third-order nonlinear susceptibility elements under different conditions. Furthermore, we explain the different contributions by the difference from combinations of transition paths for three incident beam polarization schemes. Moreover, we report the polarization characteristics of the singly dressed and doubly dressed FWM processes in either a two-level or a three-level atomic system in Na vapor. In the three-level atomic system the FWM signal generated by a linearly polarized pumping field is greatly suppressed by the dressing field, while the one generated by a circularly polarized pumping field is only slightly influenced by the dressing field. Also, different change rules are observed when the polarization of the probe field is changed. Different dressing effects of two dressing schemes are used to explain this phenomenon. The dressing effects, as well as the interference between the two coexisting FWM signals, have been discussed in different laser polarization configurations. Investigations of the interactions between different FWM processes and their polarization properties can help us to understand the underlying physical mechanisms and to effectively optimize the generated nonlinear optical signals. Controlling nonlinear optical processes can have many potential applications such as in all-optical switches [9] and quantum-information processing [10,11].

This paper is organized as follows: Section 2 we de-

scribe our experimental setup. In Section 3 we present the basic theoretic treatments about Zeeman atomic subsystems interacting with arbitrarily polarized laser fields. We will discuss the experimental results and comparisons with the theoretical calculations in Section 4. Section 6 summarizes main results and gives conclusions.

2. EXPERIMENTAL SETUP

The experiments are carried out in Na vapor (in a heat pipe oven), which is heated up to a temperature of about 235°C. Three energy levels from Na atoms are involved in the experimental schemes. As shown in Fig. 1, energy levels $|0\rangle(3s_{1/2})$ and $|1\rangle(3p_{3/2})$ form the two-level atomic system. Two laser beams E_d (ω_p, $\mathbf{k}_d$, and Rabi frequency G_d) and E_d' (ω_p, $\mathbf{k}_d'$, and Rabi frequency G_d'), connecting the transition between $|0\rangle$ and $|1\rangle$, propagate in the opposite direction of the weak probe beam E_p (ω_p, $\mathbf{k}_p$, and Rabi frequency G_p), which also connects the transition between $|0\rangle$ and $|1\rangle$. The three laser beams come from the same dye laser DL1 (wavelength of 589.0 nm, 10 Hz repetition rate, 5 ns pulse width, and 0.04 cm^{-1} linewidth) with the frequency detuning Δ_1, pumped by the second-harmonic beam of a Nd:YAG laser. These three laser fields generate a degenerate-FWM (DFWM) process satisfying the phase-matching condition of $\mathbf{k}_{s1}=\mathbf{k}_p+\mathbf{k}_d-\mathbf{k}_d'$. The energy levels $|0\rangle(3s_{1/2})-|1\rangle(3p_{3/2})-|2\rangle(4d_{3/2})$ form the cascade three-level atomic system. Two additional coupling laser beams E_c (ω_c, $\mathbf{k}_c$, and Rabi frequency G_c) and E_c' (ω_c, $\mathbf{k}_c'$, and Rabi frequency G_c'), connecting the transition between $|1\rangle$ to $|2\rangle$ are from another dye laser DL2 (which has the same characteristics as the DL1) with a frequency detuning Δ_2. E_c, E_c', and E_p fields interact with each other and generate a nondegenerate FWM (NDFWM) signal, satisfying the phase-matching condition of $\mathbf{k}_{s2}=\mathbf{k}_p+\mathbf{k}_c-\mathbf{k}_c'$. The generated DFWM and NDFWM signals propagate along slightly different directions due to their different spatial phase-matching conditions. Two photomultiplier tube (PMT) detectors are used to receive the horizontally polarized component (P polarization) and the vertically polarized component (S polarization) for one of the signal beams, or horizontally polarized components of both signal beams, respectively. A half-wave plate (HWP) and a quarter-wave plate (QWP) are selectively used (in different experiments, respectively) to control the polarization states of the incident fields. The generated FWM signals may pass through another HWP and a polarization beam splitter (PBS) before being detected by the two PMTs.

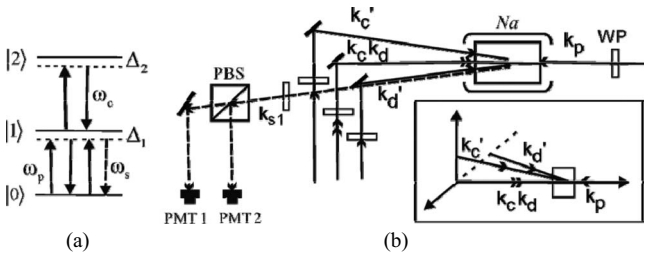

(a) (b)

Fig. 1. Schematic diagrams of the experimental arrangement and the relevant energy levels in the Na atom.

3. BASIC THEORY

A. Various Nonlinear Susceptibilities for Different Polarization Schemes

The polarization dependence of the FWM signals can be explained using either a classical or quantum mechanical description [12]. Classically, the FWM signal intensity is proportional to the square of the atomic polarization induced in the medium. For example, as for phase-conjugated FWM generation in the cascade atomic system at frequency $\omega_s=\omega_c-\omega_c+\omega_p$ (as shown in Fig. 1, with beams $\mathbf{k}_d$ and $\mathbf{k}_d'$ blocked), the nonlinear polarization along i ($i=x,y$) direction is given by

$$P_i^{(3)}(\omega_s)=\epsilon_0\sum_{jkl}\chi_{ijkl}^{(3)}(-\omega_s;\omega_c,-\omega_c,\omega_p)E_{cj}(\omega_c)E_{ck}^{*}(\omega_c)E_{pl}(\omega_p), \tag{1}$$

where $\chi_{ijkl}^{(3)}(-\omega_s;\omega_c,-\omega_c,\omega_p)$ is the tensor component of the third-order nonlinear susceptibility. For an isotropic medium like Na atomic vapor and considering that all the incident beams and signals are transverse waves, only four nonzero tensor elements are involved in this system, which are denoted as χ_{xxxx}, χ_{yxxy}, χ_{yyxx}, χ_{yxyx}. Different polarization configurations of the incident fields can involve different nonlinear susceptibility elements. For example, when we use a HWP to change the polarization of the E_p field while the other two beams are originally polarized in the horizontal direction, the probe field will have two perpendicular components: $E_{px}=E_p\,\mathrm{Cos}\,2\theta$ and $E_{py}=E_p\,\mathrm{Sin}\,2\theta$ (θ is the rotated angle of the HWP's axis from the x axis). Consequently, the polarization has two corresponding components, i.e., horizontal component $P_x^{(3)}(\omega_s)=\epsilon_0\chi_{xxxx}|E_c|^2|E_{px}|$ and perpendicular component $P_y^{(3)}(\omega_s)=\epsilon_0\chi_{yxxy}|E_c|^2|E_{py}|$. Then the effective susceptibility elements χ_x and χ_y are defined as $\chi_x=\chi_{xxxx}\cos 2\theta$ and $\chi_y=\chi_{yxxy}\sin 2\theta$. As for the other two cases with $\mathbf{k}_c$ and $\mathbf{k}_c'$ modulated by a HWP. χ_{yyxx} and χ_{yxyx} become dominant on generating FWM signals polarized in the S direction (the signals in the P direction for the three cases are all generated by χ_{xxxx}). The microscopic mechanism of nonlinear different susceptibilities will be discussed in Subsection 3.B.

If a QWP is used to modulate the incident beams, the effective nonlinear susceptibilities will be different while the excited susceptibilities are the same as in the corresponding cases with HWP modulation. Table 1 presents all the effective susceptibilities for the three-field polarization schemes.

In order to measure the polarization states of the FWM signals, a HWP and a PBS are placed in the path of the signal beam (as shown in Fig. 1). When an arbitrarily polarized field $\binom{E_x}{E_y e^{i\delta}}$ passes through the HWP+PBS combination, the detected intensities are

$$I_x=\cos^2 2\alpha|E_x|^2+|E_y|^2\sin^2 2\alpha+|E_x||E_y|\sin 4\alpha\cos\delta, \tag{2}$$

$$I_y=\sin^2 2\alpha|E_x|^2+|E_y|^2\cos^2 2\alpha-|E_x||E_y|\sin 4\alpha\cos\delta, \tag{3}$$

Table 1. Effective Nonlinear Susceptibilities for Different Laser Polarization Configurations

	$\mathbf{k}_p$, $\mathbf{k}_c$, $\mathbf{k}_c'$, P	$\mathbf{k}_p$, S	$\mathbf{k}_c$, S	$\mathbf{k}_c'$, S
HWP	$\chi_x=\chi_{xxxx}\,\mathrm{Cos}\,2\theta$	$\chi_y=\chi_{yxxy}\,\mathrm{Sin}\,2\theta$	$\chi_y=\chi_{yyxx}\,\mathrm{Sin}\,2\theta$	$\chi_y=\chi_{yxyx}\,\mathrm{Sin}\,2\theta$
QWP	$\chi_x=\chi_{xxxx}\times\sqrt{\sin^4\theta+\cos^4\theta}$	$\chi_y=\chi_{yxxy}\times\sqrt{2}\lvert\sin\theta\cos\theta\rvert^2$	$\chi_y=\chi_{yyxx}\times\sqrt{2}\lvert\sin\theta\cos\theta\rvert^2$	$\chi_y=\chi_{yxyx}\times\sqrt{2}\lvert\sin\theta\cos\theta\rvert^2$

respectively, where α is the rotation angle of the HWP from the x axis and δ is the phase difference between the two polarization [horizontal (x) and vertical (y)] components of the signal beam.

B. Nonlinear Susceptibilities for a Zeeman-Degenerate System Interacting with Polarized Fields

The polarization dependence of the FWM signals can also be described by the semi-classical treatment. It is based on the fact that there are different transition paths combinations consisting of various transitions between Zeeman sublevels for different polarization schemes [as shown in Fig. 2]. According to the experimental setup, the x axis is the original polarization direction of all the incident fields, and it is also the quantization axis. We then decompose the arbitrary field into two components: parallel to and perpendicular to the x axis, respectively. When this field interacts with atoms, the perpendicular component can be decomposed into equally left-circularly- and right-circularly-polarized components. Different polarization schemes can excite different transition paths in the Zeeman-degenerate atomic systems, and so it is necessary to take into account the Clebsch–Gordan coefficients associated with the various transitions between Zeeman sublevels in all pathways when calculating the FWM intensities. Figure 2 shows the transition schematic configurations for the Zeeman-degenerate two-level and three-level cascade systems interacting with one arbitrarily polarized and two horizontally polarized fields. Table 2 and 3 list all the perturbation chains for different cases, respectively. By considering the schematic figures and the tables, we can obtain the expressions of various density matrices corresponding to nonlinear susceptibilities for different polarization schemes.

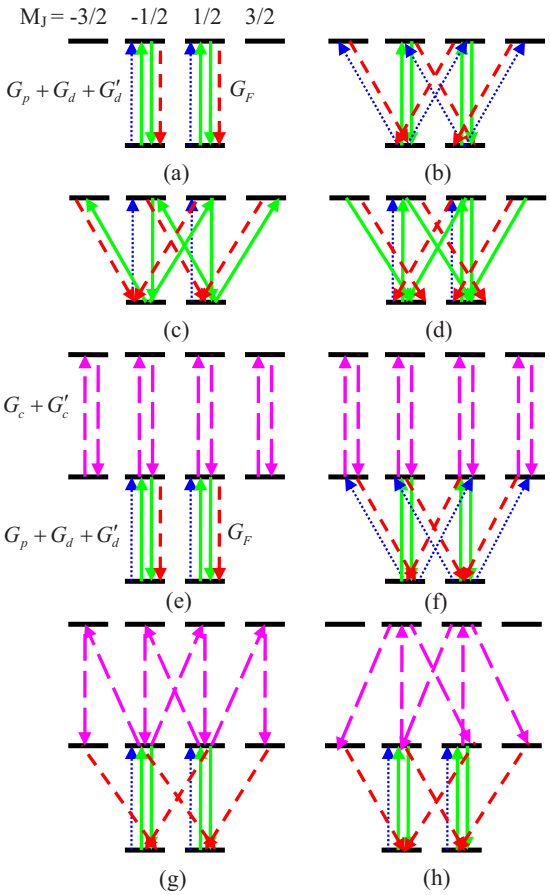

Fig. 2. (Color online) Energy level diagrams and transition paths at different laser polarization configurations. (a) and (e) Schematic diagrams of the P-polarization generation in two-level and three-level systems when the waveplates change $\mathbf{k}_p$, $\mathbf{k}_d$, and $\mathbf{k}_d'$. (b)–(d) and (f)–(h) Schematic diagrams of S-polarization generation in two-level and three-level systems when the waveplates change $\mathbf{k}_p$, $\mathbf{k}_d$, and $\mathbf{k}_d'$, respectively. Dotted, long-dashed, solid, and short-dashed lines are transitions for the probe, coupling, dressing, and FWM signal fields, respectively.

Figure 2(a) shows the configuration of generating the FWM signals in P-polarization (represented as χ_{xxxx}) in the two-level system. It contains two sub-two-level systems: $|a_{-1/2}\rangle-|b_{-1/2}\rangle$ and $|a_{1/2}\rangle-|b_{1/2}\rangle$. The respective perturbation chains are listed in Table 2 and the total contribution of these chains to the density-matrix element that induces the FWM signal in the P-polarization direction is

$$\tilde{\rho}_p^{(3)}=-i\sum_{M=\pm1/2}|G_{dM}^0|^2G_{pM}^0\left(\frac{1}{(i\Delta_p+\Gamma_{b_Ma_M})^2}+\frac{1}{\Delta_p^2+\Gamma_{b_Ma_M}^2}\right)\times\left(\frac{1}{\Gamma_{a_Ma_M}}+\frac{1}{\Gamma_{b_Mb_M}}\right). \tag{4}$$

Then from $\chi_{xxxx}=N\mu\rho_p^{(3)}/\epsilon_0|E_c|^2E_p$, we can get χ_{xxxx}.

Figure 2(b) presents the configuration for generating the S-polarized FWM signals when the waveplate (WP) changes $\mathbf{k}_p$ (corresponds susceptibility χ_{yxxy}). It contains two right-circularly-polarized V-type subsystems ($|a_{-1/2}\rangle-|b_{1/2}\rangle-|b_{-1/2}\rangle$ and $|a_{1/2}\rangle-|b_{3/2}\rangle-|b_{1/2}\rangle$), two left-circularly-polarized V-type subsystems ($|a_{-1/2}\rangle-|b_{-3/2}\rangle-|b_{-1/2}\rangle$ and $|a_{1/2}\rangle-|b_{-1/2}\rangle-|b_{1/2}\rangle$), one right-circularly-polarized reversed V-type subsystem $|a_{-1/2}\rangle-|b_{1/2}\rangle-|a_{1/2}\rangle$ and one left-circularly-polarized RV-type subsystem $|a_{1/2}\rangle-|b_{-1/2}\rangle-|a_{-1/2}\rangle$. Their perturbation chains are listed in Table 2 and the total density-matrix element including contributions from all the perturbation chains can be written as

Table 2. Perturbation Chains of the Two-Level System for Different Laser Polarization Configurations

WP change $\mathbf{k}_d$ (or $\mathbf{k}'_d$, $\mathbf{k}_p$) P polarization (χ_{xxxx})	(I) $\rho_{a_M a_M} \xrightarrow{G^0_{pM}} \rho_{b_M a_M} \xrightarrow{(G'^0_{dM})^*} \rho_{b_M b_M} \xrightarrow{G^0_{dM}} \rho_{b_M a_M}, (M = \pm 1/2).$ (II) $\rho_{a_M a_M} \xrightarrow{G^0_{pM}} \rho_{b_M a_M} \xrightarrow{(G'^0_{dM})^*} \rho_{b_M b_M} \xrightarrow{G^0_{dM}} \rho_{b_M a_M}, (M = \pm 1/2).$ (III) $\rho_{a_M a_M} \xrightarrow{(G'^0_{dM})^*} \rho_{a_M b_M} \xrightarrow{G^0_{dM}} \rho_{a_M a_M} \xrightarrow{G^0_{pM}} \rho_{b_M a_M}, (M = \pm 1/2).$ (IV) $\rho_{a_M a_M} \xrightarrow{(G'^0_{dM})^*} \rho_{a_M b_M} \xrightarrow{G^0_{dM}} \rho_{b_M b_M} \xrightarrow{G^0_{pM}} \rho_{b_M a_M}, (M = \pm 1/2).$
WP change $\mathbf{k}_p$ S polarization (χ_{yxxy})	(V-R-I) $\rho_{a_M a_M} \xrightarrow{(G'^0_{dM})^*} \rho_{a_M b_{M+1}} \xrightarrow{G^0_{dM}} \rho_{a_M a_M} \xrightarrow{G^+_{pM}} \rho_{b_{M+1} a_M}, (M = \pm 1/2).$ (V-R-II) $\rho_{a_M a_M} \xrightarrow{G^0_{dM}} \rho_{b_M a_M} \xrightarrow{(G'^0_{dM})^*} \rho_{a_M a_M} \xrightarrow{G^+_{pM}} \rho_{b_{M+1} a_M}, (M = \pm 1/2).$ (V-L-I) $\rho_{a_M a_M} \xrightarrow{G^0_{dM}} \rho_{b_M a_M} \xrightarrow{(G'^0_{dM})^*} \rho_{a_M a_M} \xrightarrow{G^-_{pM}} \rho_{b_{M-1} a_M}, (M = \pm 1/2).$ (V-L-II) $\rho_{a_M a_M} \xrightarrow{G^0_{dM}} \rho_{b_M a_M} \xrightarrow{(G'^0_{dM})^*} \rho_{a_M a_M} \xrightarrow{G^-_{pM}} \rho_{b_{M-1} a_M}, (M = \pm 1/2).$ (V-R) $\rho_{a_M a_M} \xrightarrow{G^+_{pM+1}} \rho_{b_{M+1} a_M} \xrightarrow{(G'^0_{dM+1})^*} \rho_{a_{M+1} a_M} \xrightarrow{G^0_{dM+1}} \rho_{b_{M+1} a_M}, (M = \pm 1/2).$ (RV-L) $\rho_{a_M a_M} \xrightarrow{G^-_{pM}} \rho_{b_{M-1} a_M} \xrightarrow{(G'^0_{dM})^*} \rho_{a_{M-1} a_M} \xrightarrow{G^0_{dM}} \rho_{b_{M-1} a_M}, (M = \pm 1/2).$
WP change $\mathbf{k}_d$ S polarization (χ_{yyxx})	(I) $\rho_{a_M a_M} \xrightarrow{G^0_{p_M}} \rho_{b_M a_M} \xrightarrow{(G^0_{d_M})^*} \rho_{a_M a_M} \xrightarrow{G^-_{d_M}} \rho_{b_{M-1} a_M}, (M = \pm 1/2).$ (II) $\rho_{a_M a_M} \xrightarrow{G^0_{p_M}} \rho_{b_M a_M} \xrightarrow{(G^0_{d_M})^*} \rho_{a_M a_M} \xrightarrow{G^+_{d_M}} \rho_{b_{M+1} a_M}, (M = \pm 1/2).$ (III) $\rho_{a_{-1/2} a_{-1/2}} \xrightarrow{G^0_{p-1/2}} \rho_{b_{-1/2} a_{-1/2}} \xrightarrow{(G^0_{d-1/2})^*} \rho_{a_{-1/2} a_{-1/2}} \xrightarrow{G^+_{d-1/2}} \rho_{b_{1/2} a_{-1/2}}.$ (IV) $\rho_{a_{1/2} a_{1/2}} \xrightarrow{G^0_{p1/2}} \rho_{b_{1/2} a_{1/2}} \xrightarrow{(G^0_{d1/2})^*} \rho_{a_{1/2} a_{1/2}} \xrightarrow{G^-_{d1/2}} \rho_{b_{-1/2} a_{1/2}}.$
WP change $\mathbf{k}'_d$ S polarization (χ_{yxyx})	(I) $\rho_{a_{-1/2} a_{-1/2}} \xrightarrow{G^0_{p-1/2}} \rho_{b_{-1/2} a_{-1/2}} \xrightarrow{(G'^-_{d-1/2})^*} \rho_{a_{-1/2} a_{1/2}} \xrightarrow{G^0_{d-1/2}} \rho_{b_{1/2} a_{-1/2}}$ (II) $\rho_{a_{1/2} a_{1/2}} \xrightarrow{G^0_{p1/2}} \rho_{b_{1/2} a_{1/2}} \xrightarrow{(G'^+_{d1/2})^*} \rho_{a_{-1/2} a_{1/2}} \xrightarrow{G^0_{d1/2}} \rho_{b_{-1/2} a_{1/2}}$ (III) $\rho_{a_{-1/2} a_{-1/2}} \xrightarrow{G^0_{d-1/2}} \rho_{b_{-1/2} a_{-1/2}} \xrightarrow{(G^-_{d-1/2})^*} \rho_{a_{-1/2} a_{1/2}} \xrightarrow{G^0_{p-1/2}} \rho_{b_{1/2} a_{-1/2}}$ (IV) $\rho_{a_{1/2} a_{1/2}} \xrightarrow{G^0_{d-1/2}} \rho_{b_{1/2} a_{1/2}} \xrightarrow{(G'^+_{d-1/2})^*} \rho_{a_{-1/2} a_{1/2}} \xrightarrow{G^0_{p-1/2}} \rho_{b_{-1/2} a_{1/2}}$

Table 3. Perturbation Chains of the Cascade System for Different Laser Polarization Configurations

WP change $\mathbf{k}_p$ (or $\mathbf{k}_c$, $\mathbf{k}_c'$) P polarization (χ_{xxxx})	$\rho_{a_M a_M} \xrightarrow{G^0_{pM}} \rho_{a_M b_M} \xrightarrow{G_{cM}} \rho_{a_M c_M} \xrightarrow{(G'^0_{cM})^*} \rho_{a_M b_M}, (M=\pm 1/2).$
WP change $\mathbf{k}_p$ S polarization (χ_{yxxy})	(I) $\rho_{a_M a_M} \xrightarrow{G^-_{pM}} \rho_{a_M b_{M-1}} \xrightarrow{G^0_{cM}} \rho_{a_M c_{M-1}} \xrightarrow{(G'^0_{cM})^*} \rho_{a_M b_{M-1}}, (M=\pm 1/2).$ (II) $\rho_{a_M a_M} \xrightarrow{G^+_{pM}} \rho_{a_M b_{M+1}} \xrightarrow{G^0_{cM}} \rho_{a_M c_{M+1}} \xrightarrow{(G^0_{cM})^*} \rho_{a_M b_{M+1}}, (M=\pm 1/2).$
WP change $\mathbf{k}_c$ S polarization (χ_{yyxx})	(I) $\rho_{a_M a_M} \xrightarrow{G^0_{pM}} \rho_{a_M b_M} \xrightarrow{G^-_{cM}} \rho_{a_M c_{M-1}} \xrightarrow{(G'^0_{cM})^*} \rho_{a_M b_{M-1}}, (M=\pm 1/2).$ (II) $\rho_{a_M a_M} \xrightarrow{G^0_{pM}} \rho_{a_M b_M} \xrightarrow{G^+_{cM}} \rho_{a_M c_{M+1}} \xrightarrow{(G'^0_{cM})^*} \rho_{a_M b_{M+1}}, (M=\pm 1/2).$
WP change k_c' S polarization (χ_{yxyx})	(I) $\rho_{a_M a_M} \xrightarrow{G^0_{pM}} \rho_{a_M b_M} \xrightarrow{G^0_{cM}} \rho_{a_M c_M} \xrightarrow{(G^-_{cM})^*} \rho_{a_M b_{M-1}}, (M=\pm 1/2).$ (II) $\rho_{a_M a_M} \xrightarrow{G^0_{pM}} \rho_{b_M a_M} \xrightarrow{G^0_{cM}} \rho_{c_M a_M} \xrightarrow{(G^+_{cM})^*} \rho_{b_{M+1} a_M}, (M=\pm 1/2).$

$$\tilde{\rho}^{(3)}_{s1} = -\left[\frac{iG^-_{p_{1/2}}|G^0_{d_{1/2}}|^2}{(i\Delta_p+\Gamma_{b_{-1/2}a_{1/2}})^2\Gamma_{a_{-1/2}a_{1/2}}} + \frac{iG^+_{p_{-1/2}}|G^0_{d_{-1/2}}|^2}{(i\Delta_p+\Gamma_{b_{1/2}a_{-1/2}})^2\Gamma_{a_{1/2}a_{-1/2}}}\right] - \sum_{M=\pm 1/2}\frac{2\Gamma_{b_M a_M}|G^0_{dM}|^2}{\Gamma_{a_M a_M}(\Delta_p^2+\Gamma^2_{b_M a_M})}\left[\frac{iG^+_{pM}}{(i\Delta_p+\Gamma_{b_{M+1}a_M})} + \frac{iG^-_{pM}}{(i\Delta_p+\Gamma_{b_{M-1}a_M})}\right]. \quad (5)$$

$$\tilde{\rho}^{(r)}_{s2} = -\frac{iG^0_{p_{-1/2}}G^+_{d_{-1/2}}(G^0_{d_{-1/2}})^*}{\Gamma_{a_{-1/2}a_{-1/2}}(i\Delta_p+\Gamma_{b_{-1/2}a_{-1/2}})(i\Delta_p+\Gamma_{b_{1/2}a_{-1/2}})} - \frac{iG^0_{p_{1/2}}G^-_{d_{1/2}}(G^0_{d_{1/2}})^*}{\Gamma_{a_{1/2}a_{1/2}}(i\Delta_p+\Gamma_{b_{1/2}a_{1/2}})(i\Delta_p+\Gamma_{b_{-1/2}a_{1/2}})} - \sum_{M=\pm 1/2}\frac{iG^0_{p_M}(G^0_{d_M})^*}{\Gamma_{a_M a_M}(i\Delta_p+\Gamma_{b_M a_M})}\left[\frac{G^-_{d_M}}{(i\Delta_p+\Gamma_{b_{M-1}a_M})} + \frac{G^+_{d_M}}{(i\Delta_p+\Gamma_{b_{M+1}a_M})}\right]. \quad (6)$$

When the polarization of the $\mathbf{k}_d$ field is changed by the WP, the subsystems generating FWM signals in the P-polarization direction and their expressions are the same as the ones for changing the $\mathbf{k}_p$ field. However, the configuration of generating the S-polarized FWM signal, as shown in Fig. 2(c), contains two left-circularly-polarized V-type subsystems ($|a_{-1/2}\rangle$–$|b_{-1/2}\rangle$–$|b_{-3/2}\rangle$ and $|a_{1/2}\rangle$–$|b_{1/2}\rangle$–$|b_{-1/2}\rangle$), two right-circularly-polarized V-type subsystems ($|a_{-1/2}\rangle$–$|b_{-1/2}\rangle$–$|b_{1/2}\rangle$ and $|a_{1/2}\rangle$–$|b_{1/2}\rangle$–$|a_{3/2}\rangle$), and one right-circularly-polarized RV-type subsystem ($|a_{-1/2}\rangle$–$|a_{1/2}\rangle$–$|b_{1/2}\rangle$), and one left-circularly-polarized RV-type subsystem ($|a_{-1/2}\rangle$–$|a_{1/2}\rangle$–$|b_{1/2}\rangle$). The total contribution to the third-order nonlinear density-matrix element is

Then we can obtain the nonlinear susceptibility element χ_{xyxy}.

When changing the polarization of $\mathbf{k}_d'$ field, as shown in Fig. 2(d), there are four perturbation chains as listed in Table 2. The total contribution from all the perturbation chains to the third-order nonlinear density-matrix element can be written as

$$\tilde{\rho}^{(3)}_{s3} = -\frac{4iG^0_{p_{-1/2}}G^0_{d_{1/2}}(G'^-_{d_{-1/2}})^*}{\Gamma_{a_{-1/2}a_{1/2}}(i\Delta_p+\Gamma_{b_{1/2}a_{-1/2}})(i\Delta_p+\Gamma_{b_{-1/2}a_{-1/2}})}. \quad (7)$$

This expression is simpler due to the symmetry of the configuration relative to $M=0$. Then, we can obtain element χ_{xxyy}.

For the three-level cascade-type (C3-type) system, the schematic charts are shown in Figs. 2(e)–2(h) [with dressing fields $\mathbf{k}_d$ and $\mathbf{k}_d'$ blocked], which change $\mathbf{k}_p$, $\mathbf{k}_c$, and $\mathbf{k}_c'$ fields. The corresponding perturbation chains are listed in Table 3. The expressions of the corresponding third-order nonlinear density-matrix elements are

$$\rho_p^{(3)} = -\sum_{M=\pm 1/2} \frac{iG_{pM}^0 iG_{cM}(G_{cM}^0)^*}{(i\Delta_p + \Gamma_{b_M a_M})^2 [i(\Delta_c + \Delta_p) + \Gamma_{c_M a_M}]},$$

$$\rho_{s1}^{(3)} = -\sum_{M=\pm 1/2} \frac{iG_{pM}^- |G_{cM}^0|^2}{(i\Delta_p + \Gamma_{b_{M-1} a_M})^2 ([i(\Delta_c + \Delta_p) + \Gamma_{c_{M-1} a_M}])} - \sum_{M=\pm 1/2} \frac{iG_{pM}^+ |G_{cM}^0|^2}{(i\Delta_p + \Gamma_{b_{M+1} a_M})^2 [i(\Delta_c + \Delta_p) + \Gamma_{c_{M+1} a_M}]},$$

$$\rho_{s2}^{(3)} = -\sum_{M=\pm 1/2} \frac{iG_{pM}^0 (G_{cM}'^0)^*}{(i\Delta_p + \Gamma_{b_M a_M})} \times \left[\frac{iG_{cM}^+}{(i\Delta_p + \Gamma_{b_{M+1} a_M})[i(\Delta_c + \Delta_p) + \Gamma_{c_{M+1} a_M}]} + \frac{iG_{cM}^-}{(i\Delta_p + \Gamma_{b_{M-1} a_M})[i(\Delta_c + \Delta_p) + \Gamma_{c_{M-1} a_M}]} \right],$$

$$\rho_{s3}^{(3)} = -\sum_{M=\pm 1/2} \frac{iG_{pM}^0 G_{cM}^0}{(i\Delta_p + \Gamma_{b_M a_M})[i(\Delta_c + \Delta_p) + \Gamma_{c_M a_M}]} \times \left(\frac{(G_{cM}^-)^*}{i\Delta_p + \Gamma_{b_{M-1} a_M}} + \frac{(G_{cM}'^+)^*}{i\Delta_p + \Gamma_{b_{M+1} a_M}} \right). \quad (8)$$

C. Third-Order Density-Matrix Elements in the Presence of Dressing Fields

For the case with a single dressing by the $\mathbf{k}_d$ field (with $\mathbf{k}_d'$ blocked), the density-matrix elements of the dressed FWM signals (generated in the C3 system) are given by

$$\rho_{b_M a_M}^{(3)} = -\frac{iG_{pM}^0 |G_{cM}^0|^2}{(i(\Delta_c + \Delta_p) + \Gamma_{c_M a_M})} \times \frac{1}{\left(i\Delta_p + \Gamma_{b_M a_M} + \dfrac{|G_{dM}|^2}{i(\Delta_p - \Delta_d) + \Gamma_{a_M a_M} + \dfrac{|G_{pM}^0|^2}{\Gamma_{a_M a_M}}} + \dfrac{|G_{cM}^0|^2}{i(\Delta_c + \Delta_p) + \Gamma_{c_M a_M}} \right)^2}, \quad \left(M = \pm \frac{1}{2} \right). \quad (9)$$

For the case of double dressing (with $\mathbf{k}_d$ and $\mathbf{k}_d'$ both on), the third-order nonlinear density-matrix elements can be written as

$$\rho_{b_M a_M}^{(3)} = -\frac{iG_{pM}^0 |G_{cM}^0|^2}{i(\Delta_c + \Delta_p) + \Gamma_{c_M a_M}} \times \frac{1}{\left(i\Delta_p + \Gamma_{b_M a_M} + \dfrac{2|G_{dM}|^2}{i(\Delta_p - \Delta_d) + \Gamma_{a_M a_M} + \dfrac{|G_{pM}^0|^2}{\Gamma_{a_M a_M}}} + \dfrac{|G_{cM}^0|^2}{i(\Delta_c + \Delta_p) + \Gamma_{c_M a_M}} \right)^2}, \quad \left(M = \pm \frac{1}{2} \right). \quad (10)$$

One can easily see that the multidressed fields appear in the denominator and the dressing effect is mainly caused by the strong dressing field G_d. The other two fields, however, can enhance or suppress such dressing effect. In fact, the coupling field G_c, which is denoted as sequential with G_d, generally enhances the dressed effect induced by G_d, while the probe field G_p, which is denoted as nested with G_d, generally suppresses the dressing effect [13].

4. RESULTS AND DISCUSSIONS

First, we use a HWP to modulate the polarization of one of the incident beams, while the other two beams are kept to be in horizontally polarization. In this case, the incident beams are all linearly polarized. Figures 3(a) and 3(b) show the relative FWM intensities in the P and S polarizations, respectively, in the cascade three-level atomic system with respect to the rotation angle θ of the HWP. From Table 1 we can see that, for the horizontally polarized component [Fig. 3(a)], the dependence of the FWM intensity on θ follows $(\cos 2\theta)^2$ while the vertically polarized component obeys $(\sin 2\theta)^2$ (represented by the solid curves in Fig. 3). This means that the FWM signals are linearly polarized. Similar results have been reported in other systems [2,4,6]. From Fig. 3(b), the signal amplitudes are different for the three laser polarization configurations, which can be attributed to different contributions from the third-order nonlinear susceptibility

elements under different conditions. As discussed in Section 3, different polarization schemes of incident fields can excite different nonlinear susceptibilities, and they can have different quantum transition paths. When the $\mathbf{k}_p$ field is modulated by the HWP, χ_{yxxy} is excited, which generates FWM signal in the S-polarization direction. In the other two cases, both the $\mathbf{k}_c$ and $\mathbf{k}_c'$ fields are modulated, so both χ_{yyxx} and χ_{yxyx} are respectively stimulated. The signal amplitudes indicate different contributions from third-order nonlinear susceptibility elements for three different laser polarization schemes.

Figures 3(c) and 3(d) depict the polarization dependences of the FWM signals on the rotation angle of the QWP in the two-level DFWM process. First, the probe beam $\mathbf{k}_p$ is elliptically polarized and the ellipticity is controlled by the QWP, while the other beams have linear polarization along the x axis [the square points in Figs. 3(c) and 3(d)]. In Figs. 3(c) and 3(d), the experimental results are well described by the functions $\sin^4\varphi+\cos^4\varphi$ and $2(\sin\varphi\cos\varphi)^2$ (the solid curves), respectively. If one of the incident beams is elliptically polarized, the generated FWM signal is also elliptically polarized, which is in good agreement with the theoretical prediction. Comparing the vertically polarized intensities of the signal beams [Figs. 2(b) and 2(d)], there are different ratios of oscillation amplitudes. It indicates that the ratios of the third-order nonlinear susceptibility elements are different for the cascade three-level system and the two-level system, which are well described by Eq. (8).

To detect the polarization states of the FWM signals, we place a HWP+PBS combination as a polarization analyzer in the generated FWM signal beam (as shown in Fig. 1). In fact, when a QWP is used to modulate the $\mathbf{k}_c$ field's polarization (or ellipticity ϵ), the polarizations of the FWM signals are also changed. Besides, the excited nonlinear susceptibilities of the P and S polarizations greatly modify the signal's polarization states, which can be detected by the HWP+PBS combination. Figure 4 presents the detected results. Each curve is obtained by rotating the HWP while keeping the QWP in the path of the $\mathbf{k}_c$ field fixed. In this case, $|E_x|\propto\chi_{xxxx}\sqrt{\sin^4\theta+\cos^4\theta}$ and $|E_y|\propto\chi_{yyxx}\sqrt{\sin^2\theta\cos^2\theta}$. According to Eqs. (2) and (3), the detected intensities should be

$$
\begin{aligned}
I_x &= \chi_{xxxx}^2(\cos^4\theta+\sin^4\theta)\cos^2 2\alpha \\
&\quad + \chi_{yyxx}^2(2\sin^2\theta\cos^2\theta)\sin^2 2\alpha \\
&\quad + \chi_{xxxx}\chi_{yyxx}\sqrt{(\cos^4\theta+\sin^4\theta)(2\sin^2\theta\cos^2\theta)}\sin 4\alpha\cos\delta, \\
I_y &= \chi_{xxxx}^2(\cos^4\theta+\sin^4\theta)\sin^2 2\alpha \\
&\quad + \chi_{yyxx}^2(2\sin^2\theta\cos^2\theta)\cos^2 2\alpha \\
&\quad - \chi_{xxxx}\chi_{yyxx}\sqrt{(\cos^4\theta+\sin^4\theta)(2\sin^2\theta\cos^2\theta)}\sin 4\alpha\cos\delta.
\end{aligned}
\tag{11}
$$

If the $\mathbf{k}_c$ field is linearly polarized ($\theta=0$, $\epsilon=1$, the square points in Fig. 4), the NDFWM signal is also linearly polarized, and the horizontal (x) and vertical (y) signal intensities obey the relations of $\chi_{xxxx}^2\cos^2 2\alpha$ and $\chi_{xxxx}^2\sin^2 2\alpha$, respectively. When the polarization of the $\mathbf{k}_c$ field is changed, the other nonlinear susceptibility components are excited and the FWM signal is then elliptically polarized. From Fig. 4 we can see that, if the $\mathbf{k}_c$ field is either elliptically ($\theta=30°$, $\epsilon=0.5$, the triangle points) or circularly ($\theta=45°$, $\epsilon=0$, asterisk points) polarized, the NDFWM signals are also elliptically polarized. This can be confirmed by Eq. (11). When the input $\mathbf{k}_c$ field is circularly polarized, the FWM signal can be circularly polarized once the condition $\chi_{xxxx}=\chi_{yyxx}$ is satisfied.

Figure 5 shows the dependence of the dressed FWM signal on the polarization of the $\mathbf{k}_c$ field. Figures 5(a) and 5(b) depict the results for the $\mathbf{k}_d$ singly-dressed and $\mathbf{k}_d$ and $\mathbf{k}_d'$ doubly dressed FWM signals, respectively, for three different ellipticities of the $\mathbf{k}_c$ field. The dressing fields $\mathbf{k}_d$ and $\mathbf{k}_d'$ are both linearly polarized along the x axis. Comparing to Fig. 4(a), the reduction of the signal intensity is more than 50%. More interestingly, the FWM signals generated by the linearly polarized $\mathbf{k}_c$ field [the square points in Fig. 4(a) and Fig. 5(a)] are greatly suppressed by the $\mathbf{k}_d$ dressing field while the FWM signals

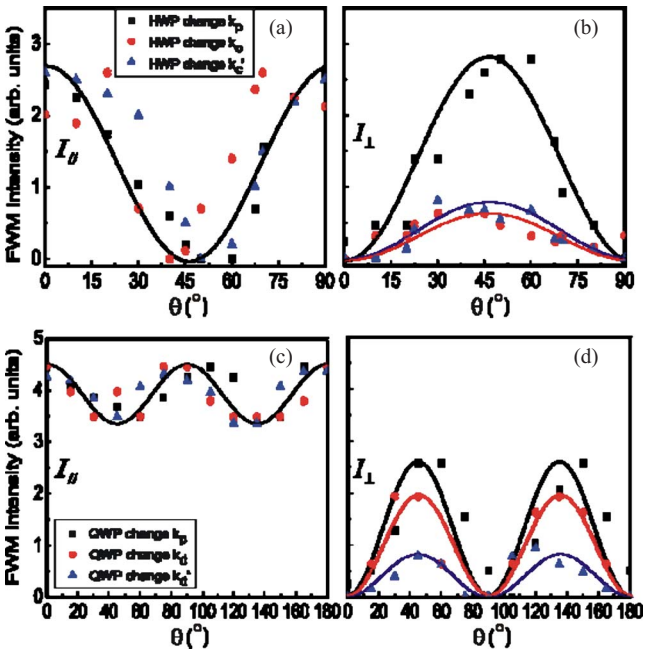

Fig. 3. (Color online) Variations of the relative FWM intensities versus the rotation angle of the waveplate. (a) and (b) The FWM signals of the cascade three-level system with the HWP. (c)–(d) The FWM signals of the two-level system with the QWP. The scattered points are the experimental data and the solid curves are the theoretical results.

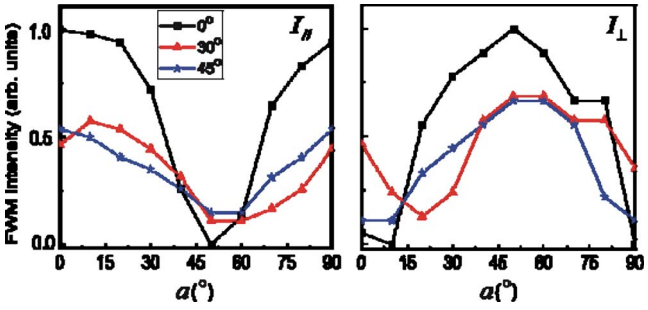

Fig. 4. (Color online) Dependence of the relative NDFWM signal intensity on α for three values of the coupling laser's ellipticity.

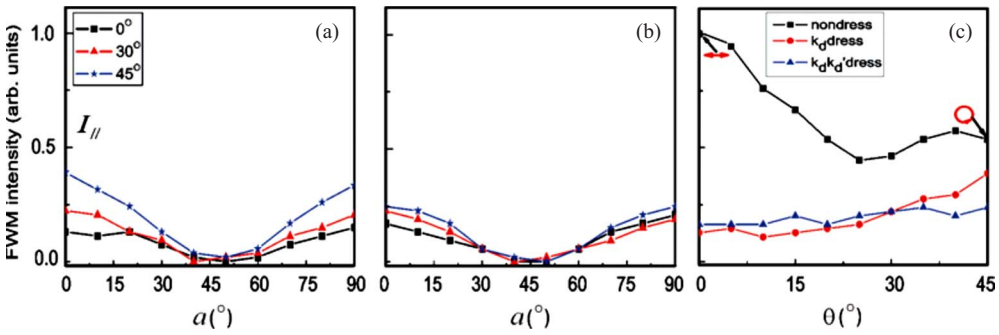

Fig. 5. (Color online) Variations of the dressed NDFWM signal intensities versus α. (a) Singly dressed FWM signals when the coupling beam $\mathbf{k}_c$ is modulated by the QWP. (b) Doubly dressed FWM signals when the coupling beam $\mathbf{k}_c$ is modulated by the QWP. (c) Variation of the relative FWM intensity versus the rotation angle θ of the QWP.

generated by the circularly polarized $\mathbf{k}_c$ field [the asterisk points in Fig. 4(a) and Fig. 5(a)] are only slightly suppressed by the $\mathbf{k}_d$ dressing field. So, in Fig. 5(a) the square points are lower than the other curves, which is opposite to the case in Fig. 4(a). Figure 5(c) presents the dependences of the pure FWM and dressed FWM signal intensities on the ellipticity of the $\mathbf{k}_c$ field. The square points represent pure FWM case, which decreases as the $\mathbf{k}_c$'s ellipticity reduces [from 1 to 0 when the QWP is rotated from 0 to 45 degrees]. The dot points represent the singly dressed FWM case, which shows an opposite variation from the pure FWM. This result can be explained by the expression [Eq. (9)] for the dressed FWM case. In the denominator of Eq. (9), G_d's sequential dressing field G_c can enhance the dressing effect. When the coupling field is linearly polarized, its Rabi frequency G_c in the denominator is at its maximum, so the dressing effect is strongest [square points in Fig. 5(a)] and the FWM signal is lowest.

Moreover, comparing the singly dressed and doubly dressed FWM signals, they have similar suppressed intensities when the signals are linearly polarized. However, when the signals are elliptically polarized, the suppression in the doubly dressed case is stronger than in the singly dressed case. In order to explain this effect, mutual-dressing processes and constructive or destructive interference between the two coexisting FWM channels should be considered [14,15]. According to Eqs. (9) and (10), if one only considers the dressing effect, the FWM intensity should be further suppressed in the doubly dressed configuration. However, as can be seen from Fig. 1, when five laser beams are all on, the DFWM signal $\mathbf{k}_{s1}$ and the NDFWM signal $\mathbf{k}_{s2}$ coexist in the experiment, and these two FWM signals overlap in frequency and the angle between their propagation directions is very small. As mentioned above, if the incident beams are all linearly polarized, the generated FWM signals are linearly polarized also, so constructive or destructive interference can occur in this system. Such interferences between two FWM processes in the two-level and three-level atomic systems can generate entangled photon pairs [16,17]. Constructive or destructive interference can be controlled by the phase difference between the two FWM processes, which can be varied by adjusting the detuning difference $\Delta(\Delta=\Delta_1-\Delta_2)$ between the incident laser beams. By varying the detuning difference Δ from 0 to very certain values, the phase difference between the two FWM processes alters from in-phase to out-phase, so the interference can switch back and forth between constructive and destructive values [18–20]. In this case, the observed experimental data include two contributions: the dressing effect and the interference effect. However, when the $\mathbf{k}_c$ field is elliptically or circularly polarized, the NDFWM signal $\mathbf{k}_{s2}$ is elliptically polarized, but the DFWM signal $\mathbf{k}_{s1}$ is still linearly polarized. In this case, the doubly dressed effect plays a dominant role to further suppress the intensity of the generated FWM signal.

The dependences of the dressing effects on the polarization of the probe field are shown in Fig. 6. Compared to Fig. 5(a), the linearly polarized signal (square points) is higher than the other curves even though it is also dressed. Such opposite behaviors in changing the pumping field $\mathbf{k}_c$ and the probe field $\mathbf{k}_p$ can be accounted for by Eq. (9). In the denominator of the equation, the dressing field G_d and the coupling field G_c are in summation form, which is called sequential-dressing scheme, and G_d and G_p are in the nest-dressing scheme [13]. According to the interaction properties of the two dressing schemes, the sequentially dressing G_c field controls the FWM process directly, which can enhance the G_d dressing effect. When the coupling field is linearly polarized, the Rabi frequency G_c in the denominator is at its maximum, so the dressing effect is strongest [square points in Fig. 5(a)]. As G_p is nested with G_d, it controls the FWM process only indirectly and it often suppresses the G_d dressing effect, so for the linearly polarized $\mathbf{k}_p$ field, the signal [square points in Fig. 6(b)] is higher than the other curves.

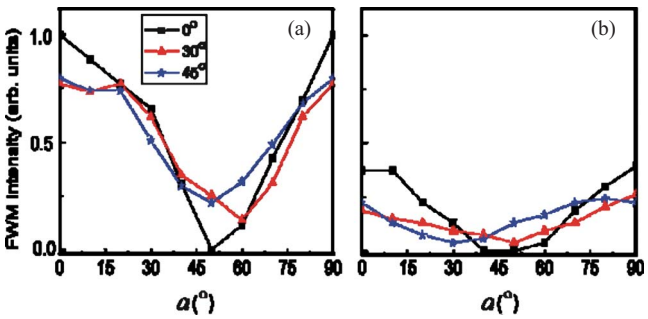

Fig. 6. (Color online) Dependence of the relative NDFWM signal intensity on α for three values of probe laser's ellipticity. (a) and (b) Pure and singly dressed FWM signals, respectively, of the cascade three-level system as the probe beam is modulated by the QWP.

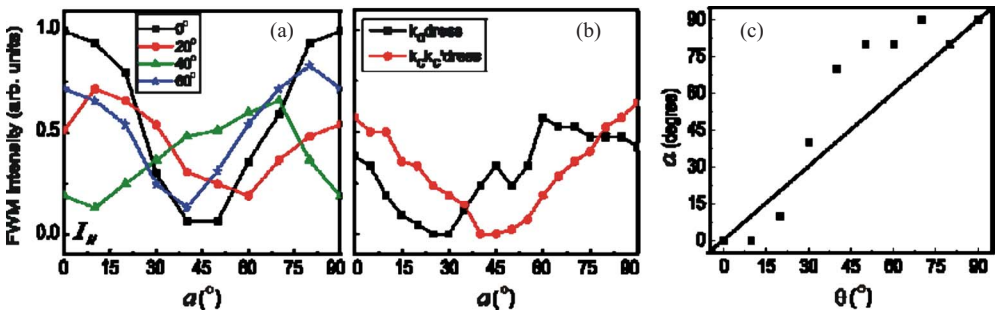

Fig. 7. (Color online) Variations of the DFWM signal intensities versus α (a) Pure FWM signal of the two-level system versus α for several different rotation angles θ of the HWP. (b) Singly dressed and doubly dressed FWM signals when the input beams are all horizontally polarized. (c) The rotation angle α of the polarization analyzer when the maximum intensity is observed. The scattered points are the experimental results, and the solid line represents the case with the polarization analyzer and polarizer rotating the same angle ($\alpha=\theta$).

Figure 7(a) depicts the dependence of the horizontal intensity of the FWM signal on α generated in the two-level system when the probe beam $\mathbf{k}_p$ is modulated by the HWP. In this case, the generated FWM signals are linearly polarized ($\delta=0$), with $|E_x| \propto \chi_{xxxx} \cos 2\theta$ and $|E_y| \propto \chi_{yxxy} \sin 2\theta$. From Fig. 7(a), with a rotating HWP, the maximal values of the curves are shifted, which indicates that the polarization of the FWM signal changes with that of the probe beam. Previous experiment [4] in rubidium vapor has shown that the polarizations of the driving field and the signal wave are identical and collinear.

If the signal and the probe beams are polarized along the same direction, a maximum signal intensity is observed when the two HWPs are rotated to be at the same angle [that is, $\alpha=\theta$, the solid line in Fig. 7(c)]. The experimental results (the scattered points) in Fig. 7(c) present a big difference from the solid theoretical line, which suggests that the signal and the probe beams have different polarization directions. According to Eqs. (2) and (3), the polarization of the FWM signal is dependent on the ratio χ_{yxxy}/χ_{xxxx}. If $\chi_{yxxy}=\chi_{xxxx}$, the signal and the probe beams would have polarization along the same direction. However, our theoretical expressions [Eq. (4) and Eq. (5)], indicate that $\chi_{yxxy} \neq \chi_{xxxx}$, so the signal and the probe beams have different polarization directions.

Figure 7(b) presents the $\mathbf{k}_c$ singly dressed (the square points) and $\mathbf{k}_c$ and $\mathbf{k}_c'$ doubly dressed (the dot points) DFWM signals when the input beams ($\mathbf{k}_d$, $\mathbf{k}_d{}'$, $\mathbf{k}_p$, $\mathbf{k}_c$, and $\mathbf{k}_c'$) are all horizontally polarized. Compared with the pure-FWM signal [the square points in Fig. 7(a)], the two FWM signals dressed by either $\mathbf{k}_c$ or $\mathbf{k}_c$ and $\mathbf{k}_c'$ are both significantly suppressed and have similar suppressed intensities. As discussed above, for the $\mathbf{k}_c$ and $\mathbf{k}_c'$ doubly dressed FWM process, the mutual-dressing effect and constructive or destructive interference should also be considered simultaneously.

5. CONCLUSION

The polarization dependences of the DFWM and NDFWM processes, and their dressing effects in two-level and three-level cascade-type atomic systems are investigated experimentally and theoretically. The effective nonlinear susceptibilities and the corresponding combinations of different transition paths for various laser polarization configurations are analyzed in detail. The polarizations of the generated FWM signals depend on both the input laser polarizations and the excited nonlinear susceptibility elements of the atomic systems. In the singly dressed FWM processes, we found that the dependences of dressing effects on the polarizations of the pumping and probe fields are very different. The FWM signal generated by the linearly polarized pumping field $\mathbf{k}_c$ is strongly dressed by the $\mathbf{k}_d$ field while the FWM signal generated by the circularly polarized $\mathbf{k}_c$ is weakly dressed by the $\mathbf{k}_d$ field, but the opposite behavior was seen for changing the polarization of the probe field. Such behavior is attributed to different dressing effects of the sequential-dressing scheme and the nest-dressing scheme. For the doubly dressed process, the polarization dependence of the signal intensity is also investigated. It is found that when the two coexisting FWM signals have the same polarization, the suppressed intensities of the singly dressed and doubly dressed signals are similar. In this case, both the mutual-dressing effects and the constructive or destructive interference should be considered simultaneously. However, when the two FWM signals have different polarizations, the doubly dressed effect plays a dominant role, so the doubly dressed signals are further suppressed. Studying polarization dependence of the FWM processes in multilevel atomic systems can be very important in optimizing and controlling nonlinear optical processes, and for various potential applications in nonlinear signal processing.

ACKNOWLEDGMENTS

This work was supported by the National Natural Science Foundation of China (NSFC) (No. 60678005), the Foundation for the Author of National Excellent Doctoral Dissertation of China (No. 200339), the Specialized Research Fund for the Doctoral Program of Higher Education of China (No. 20050698017), the Fok Ying-Tong Education Foundation for Young Teachers in the Institutions of Higher Education of China (No. 101061), and the Program for New Century Excellent Talents in University (NCET-08–0431).

REFERENCES

1. K. Tsukiyama, "Parametric four-wave mixing in Kr," J. Phys. B **29**, L345–L351 (1996).
2. L. Museur, C. Olivero, D. Riedel, and M. C. Castex, "Polarization properties of coherent VUV light at 125 nm generated by sum-frequency four-wave mixing in mercury," Appl. Phys. B **70**, 499–503 (2000).
3. J. Ishii, Y. Ogi, Y. Tanaka, and K. Tsukiyama, "Observation of the two-photon resonant parametric four-wave mixing in the NO $C^2\Pi$ ($v=0$) state," Opt. Commun. **132**, 316–320 (1996).
4. C. J. Zhu, A. A. Senin, Z. H. Lu, J. Gao, Y. Xiao, and J. G. Eden, "Polarization of signal wave radiation generated by parametric four-wave mixing in rubidium vapor: Ultrafast ($\sim$150-fs) and nanosecond time scale excitation," Phys. Rev. A **72**, 023811 (2005).
5. P. B. Chapple, K. G. H. Baldwin, and H. A. Bachor, "Interference between competing quantum-mechanical pathways for four-wave mixing," J. Opt. Soc. Am. B **6**, 180–183 (1998).
6. W. C. Magno, R. B. Prandini, P. Nussenzveig, and S. S. Vianna, "Four-wave mixing with Rydberg levels in rubidium vapor: Observation of interference fringes," Phys. Rev. A **63**, 063406 (2001).
7. W. R. Garret and Y. Zhu, "Coherent control of multiphoton driven processes: A laser-induced catalyst," J. Chem. Phys. **106**, 2045–2048 (1997).
8. Y. Wu, J. Saldana, and Y. F. Zhu, "Large enhancement of four-wave mixing by suppression of photon absorption from electromagnetically induced transparency," Phys. Rev. A **67**, 013811 (2003).
9. H. Ma, A. S. L. Gomes, and Cid B. de Araujo, "All-optical power-controlled switching in wave mixing: application to semiconductor-doped glasses," Opt. Lett. **18**, 414–416 (1993).
10. N. Gisin, G. Ribordy, W. Tittel, and H. Zbinden, "Quantum cryptography," Rev. Mod. Phys. **74**, 145–195 (2002).
11. T. B. Bahder and P. A. Lopata, "Fidelity of quantum interferometers," Phys. Rev. A **74**, 051801(R) (2006).
12. S. S. Vianna, P. Nussenzveig, W. C. Magno, and J. W. R. Tabosa, "Polarization dependence and interference in four-wave mixing with Rydberg levels in rubidium vapor," Phys. Rev. A **58**, 3000–3003 (1998).
13. Z. Q. Nie, H. B. Zheng, P. Z. Li, Y. M. Yang, Y. P. Zhang, and M. Xiao, "Interacting multi-wave mixing in a five-level folding atomic system," Phys. Rev. A **77**, 063829 (2008).
14. H. B. Zheng, Y. P. Zhang, Z. Q. Nie, C. B. Li, H. Chang, J. P. Song, and M. Xiao, "Interplay among multidressed four-wave mixing processes," Appl. Phys. Lett. **93**, 241101 (2008).
15. Y. P. Zhang, B. Anderson, A. W. Brown, and M. Xiao, "Competition between two four-wave mixing channels via atomic coherence," Appl. Phys. Lett. **91**, 061113 (2007).
16. S. G. Du, J. M. Wen, M. H. Rubin, and G. Y. Yin, "Four-wave mixing and biphoton generation in a two-level system," Phys. Rev. Lett. **98**, 053601 (2007).
17. S. G. Du, E. Oh, J. M. Wen, and M. H. Rubin, "Four-wave mixing in three-level systems: Interference and entanglement," Phys. Rev. A **76**, 013803 (2007).
18. Y. P. Zhang and M. Xiao, *Multi-Wave Mixing Processes* (Higher Education Press, Beijing and Springer, Berlin, 2009).
19. Y. P. Zhang, A. W. Brown, and M. Xiao, "Opening four-wave mixing and six-wave mixing channels via dual induced transparency," Phys. Rev. Lett. **99**, 123603 (2007).
20. Y. P. Zhang, U. Khadka, B. Anderson, and M. Xiao, "Temporal and spatial interference between four-wave mixing and six-wave mixing channels," Phys. Rev. Lett. **102**, 013601 (2009).